Macromolecules
Cite This: Macromolecules XXXX, XXX, XXX–XXX
Article
pubs.acs.org/Macromolecules

Crystallization and Molecular Topology of Linear Semicrystalline Polymers: Simulation of Uni- and Bimodal Molecular Weight Distribution Systems

Zengqiang Zhai, Julien Morthomas, Claudio Fusco, Michel Perez, and Olivier Lame*

Univ de Lyon, INSA Lyon, MATEIS, UMR CNRS 5510, 69621 Villeurbanne, France

ABSTRACT: The crystallization behavior and the molecular topology of bimodal molecular weight distribution (MWD) polymers are studied using a coarse-grained molecular dynamics model with varying weight fraction of short and long chains. Extensive simulations have been performed to prepare polymer melts and obtain semicrystalline polymers by homogeneous isothermal crystallization. The incubation time (the time elapsed before the establishment of steady-state nucleation) is calculated, and the interfacial free energy is obtained using a mean first-passage time analysis. The incubation time first decreases with the weight fraction of long chains, reaches its maximum at 30%, and then increases. This results from the conflicting effects of interfacial free energy and mobility of chain segments. The interfacial free energy decreases with the weight fraction of long chains, which is attributed to the transition from intermolecular to intramolecular nucleation, whereas the chain mobility decreases with increasing long-chain content. Nevertheless, the growth rate of crystals decreases continuously with the weight fraction of long chains, mainly resulting from reduced chain sliding diffusion. We have provided insights into how bimodal MWD polymers promote both nucleation and processability. Moreover, a numerical algorithm has been proposed, tracing each chain going back and forth among crystallites, to access quantitative data of molecular topology (i.e., loop, tie, and cilia segments). It turns out that the concentration of loop and tie segments increases with the increasing weight fraction of long chains. This could be important to understand the mechanical properties of semicrystalline polymers.

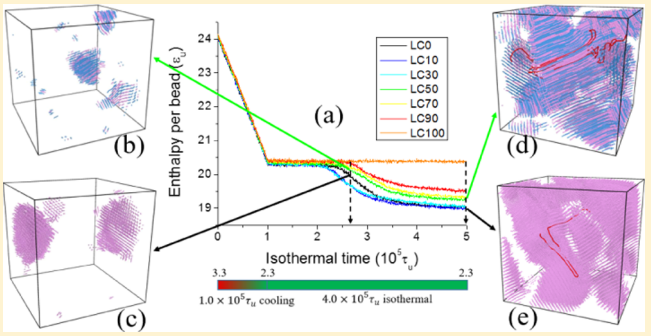

1. INTRODUCTION

Nanostructured polymers such as semicrystalline polymers are used in a broad range of applications.[1,2] Earlier studies have shown that the molecular topology of the amorphous phase is extremely important for the tensile or compression behavior of semicrystalline polymers, the fracture toughness, and the resistance to slow crack growth.[3−5] Molecular topology is characterized by the number density of (i) tie chain segments that span the interlamellar region and connect two different crystallites, (ii) loop segments that start from one crystallite and then fold back into the same one, and (iii) cilia segments that start from one crystal face and end in the amorphous region.[6,7] Such topological features and the alternation of crystalline and noncrystalline domains have formed the basis of most molecular-level description of the semicrystalline state.[8,9] Earlier works[10−12] have reported that among all the possible molecular topologies, tie segments, linking two adjacent crystallites, are supposed to contribute most effectively to the mechanical behavior of semicrystalline polymers.

The probability that different segments of a given chain are incorporated into separate lamellae forming tie segments depends on the length scale of the chain in the molten state relative to the interlamellar distance. Huang and Brown's statistical approach appears to be the most appropriate one for the assessment of tie molecules (TMs) and has aroused much interest.[4,13,14] Experimental investigations[4,15−17] have also inferred that molecular weight distribution (MWD) is a key factor for the formation of TMs. Nevertheless, unimodal MWD polymers made by traditional catalysis have conflicts between their mechanical properties and processing behaviors: improving mechanical performances by increasing the molecular weight (M_w) usually deteriorates the processability because of high melt viscosity.

More recently, thanks to the development of some novel synthetic techniques, polymers with bimodal MWD have been drawing an increasing attention, for instance, the application of bimodal polyethylene (PE) for the transportation and distribution of water and gas. The bimodal MWD material consisting of both the high-molecular-weight fraction and low-molecular-weight fraction provides more balanced performances for processing and mechanical behaviors because the low-molecular-weight polymer chains promote the melt to flow easily, whereas the high-molecular-weight fraction improves the mechanical properties of the material.[18] At present, there

Received: January 12, 2019
Revised: April 23, 2019

DOI: 10.1021/acs.macromol.9b00071
Macromolecules XXXX, XXX, XXX–XXX

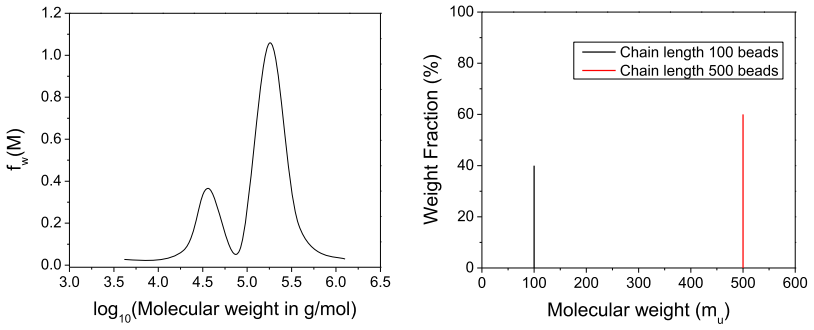

Figure 1. (a) Density distribution, $f_w(M_w)$, as a function of the logarithm of chain molecular weight, $\log(M_w)$, for the polybutadiene binary blend (from ref 38). (b) Binary polymer model proposed in this work.

are two methods for directly producing bimodal resins: reactor in series configuration or single reactor with dual-site catalysts.[6,19] Generally, it is difficult and expensive to directly prepare bimodal resins in the laboratory.[20,21] A melt blending is better suited to prepare a series of bimodal MWD polymers with variable molecular weight.[22,23] For bimodal MWD polymers, the research mainly focuses on the synthetic techniques and characterization compared to unimodal polymers.[2,24,25] However, no experimental technique allows to directly obtain quantitative data for the tie molecule concentration or topology or to evaluate their exact contribution to the mechanical behavior. The molecular topology is therefore evaluated only indirectly by mechanical testing,[3,26] molecular simulation,[6,27] or statistical analysis.[2,28−30] Furthermore, the crystallization behavior of bimodal MWD polymers has rarely been reported,[20,21,31] and the influence of the MWD on the final molecular topology of the obtained semicrystalline polymer has not been investigated.

The united-atom (UA) model and coarse-grained (CG) model are widely used in the simulation of polymer crystallization. UA dynamic simulations[32,33] have been performed for short-chain (20 methylene units) systems, and it is found that an ordered phase was formed after the induction period. However, the induction period was not quantitatively provided in these works. The UA model is mainly used with relatively short chain systems, and it is not sufficient to simulate the growth of large lamellae. In the CG model, the size of the system and the time scale involved are large enough to fully address the problems of the size, thickness, and shape of the lamellae as well as the molecular topology. CG molecular dynamics (CG-MD) is also an excellent tool to overcome difficulties of experimental measurements and to study quantitatively the nonequilibrium process of crystallization at the nanoscale. There are only a couple of reports on bimodal MWD using Monte Carlo (MC) simulation focused on polymerization.[34−36] To the best of the authors' knowledge, very few CG-MD studies focus on the effect of a bimodal MWD on the molecular topology and/or mechanical properties. In this work, seven uni- and bimodal MWD polymer systems have been prepared using CG-MD. Extensive simulations of isothermal crystallization have been performed, the nucleation behavior and crystal growth have been investigated, and the final influence on the molecular topology of the obtained semicrystalline polymer has been addressed.

Section 2 presents the simulation methods and the technique for the analysis of the topology. The results for isothermal crystallization, nucleation, and molecular topology are discussed in Section 3. Section 4 is devoted to conclusions and perspectives.

2. METHODOLOGY

We use a CG polymer model[28] where polymer chains consist of "beads" representing a few structural units. All simulations are performed in three dimensions using the open-source code LAMMPS.[37]

2.1. Interaction Potentials. The model is based on two potentials, where energy, length, and time units are given by ϵ_u, σ_u, and τ_u, respectively (with $\tau_u = \sqrt{m_u {\sigma_u}^2/\epsilon_u}$, where m_u is the mass unit). A finite-extensible nonlinear elastic (FENE) potential models intrachain interactions of bonded beads

$$V_{\mathrm{FENE}}(r) = -0.5kR_0{}^2 \ln\left[1 - \left(\frac{r}{R_0}\right)^2\right] + 4\varepsilon\left[\left(\frac{\sigma_F}{r}\right)^{12} - \left(\frac{\sigma_F}{r}\right)^{6}\right] \quad (1)$$

with $k = 30\epsilon_u/{\sigma_u}^2$, $R_0 = 1.5\sigma_u$, $\epsilon = 1\epsilon_u$, and $\sigma_F = 1.05\sigma_u$. Note that the value of σ_F is chosen such that $V_{\mathrm{FENE}}(r = 1\sigma_u)$ is minimum. All other interactions are modeled by a simple Lennard-Jones (LJ) potential

$$V_{\mathrm{LJ}}(r) = 4\epsilon\left[\left(\frac{\sigma}{r}\right)^{12} - \left(\frac{\sigma}{r}\right)^{6}\right] - 4\epsilon\left[\left(\frac{\sigma}{r_c}\right)^{12} - \left(\frac{\sigma}{r_c}\right)^{6}\right] \quad (2)$$

where $\epsilon = 1\epsilon_u$, $r_c = 2.5\sigma\sigma_u$ is the cutoff radius, and σ is an adjusted parameter of the potential that favors crystallization and crystal stability for the FENE−LJ model chosen here. We take $\sigma_{LJ} = 1.888\sigma_u$ as proposed in our previous work,[28] where the polymer chains tend to align and form thermal stable crystallites. In this LJ potential, σ_{LJ} is approximately twice the bond length ($c = 0.995$). There is a large repulsive sphere which pushes the beads to be aligned for the low-energy purpose. In fact, the simple LJ potential acts as an angular potential that helps to align the beads in the same chain.

2.2. Modeling Systems. As indicated in Figure 1a, experimental bimodal MWD polymers have two dominating chain lengths: a longer one and a shorter one. In order to mimic a real bimodal MWD polymer, we incorporate in our CG-MD simulations two types of chains: long chains with 500 units and short chains with 100 units (Figure 1b). To investigate the isothermal crystallization mechanism of

DOI: 10.1021/acs.macromol.9b00071
Macromolecules XXXX, XXX, XXX−XXX

polymers and get insights into the strength of bimodal MWD polymers, we have created seven systems of uni- and bimodal MWD polymers with varying weight fraction of long chains. For the record, there is the same total number of units in the seven systems, that is, 100 000 (see Table 1).

Table 1. Seven Modeling Systems of Uni- and Bimodal MWD Polymers: Long-Chain Length Is 500 Units and Short-Chain Length Is 100

systems	number of long chains	number of short chains	weight fraction of long chains (%)	average molecular weight ($\overline{M_w}/m_u$)
LC0	0	1000	0	100
LC10	20	900	10	108.7
LC30	60	700	30	131.6
LC50	100	500	50	166.7
LC70	140	300	70	227.3
LC90	180	100	90	357.1
LC100	200	0	100	500

2.3. Simulation Procedure. *2.3.1. Preparation of the Polymer Melts.* Polymer chains have been generated and equilibrated using the radical-like polymerization method.[39,40] This method starts with a LJ bath of N_{mon} monomers, with M of them being radicals. At each growth step, each radical forms a bond with a new monomer and transfers the radical to the chosen monomer. At the end of the method, M chains of N units are formed (for details, see our previous work[40]). The system is then equilibrated during $5 \times 10^5 \tau_u$ at $T = 3.3\epsilon_u/k_B$ and $P = 0.5\epsilon_u/\sigma_u^3$ in the *NPT* ensemble. Mean-square internal distance (MSID), radius of gyration, and end-to-end distance are calculated to verify that all systems are well equilibrated, as it will be demonstrated in Section 3.1 for the MSID. In this way, we have created seven systems of uni- and bimodal MWD polymer melts with targeted chain length as indicated in Table 1.

2.3.2. Isothermal Crystallization. After the preparation of polymer melts, isothermal crystallization study has been carried out on the seven systems according to the following procedure: starting from an equilibrated melt at $T = 3.3\epsilon_u/k_B$, where it was verified that no crystallization occurs, the temperature is cooled down to the desired crystallization temperature of $2.3\epsilon_u/k_B$ during $10^5\tau_u$ (cooling rate: $10^{-5}\epsilon_u/k_B/\tau_u$) and maintained during $4 \times 10^5\tau_u$. In our previous work,[28] this isothermal temperature ($2.3\epsilon_u/k_B$) has been chosen after an extensive test campaign in order to maximize the size of the crystallites and induce a fast growth of crystallites.

2.4. Classical Nucleation Theory and Mean First-Passage Time Method. Classical nucleation theory (CNT) method has been widely used to describe homogeneous nucleation. In semicrystalline polymers, two types of crystal interfaces with the melt are formed: chain-end or chain-folded surface and side surface. For this reason, a cylinder model is often assumed to describe the shape of nuclei. The free energy of formation of a cylindrical crystal nucleus is given by

$$\Delta G = 2\pi r^2 \sigma_e + 2\pi r l \sigma_s - \pi r^2 l \Delta G_v \tag{3}$$

where σ_s and σ_e are the interfacial free energies for the side and end surfaces of a cylindrical nucleus of radius r and length l and ΔG_v is the Gibbs free energy difference per unit volume between the crystal and melt phases. For deep supercooling, an approximation of ΔG_v is[41,42]

$$\Delta G_v \approx \rho_n \Delta H_f T(T_m - T)/{T_m}^2 \tag{4}$$

where ρ_n is the bead number density and ΔH_f is the melting heat per bead at the thermodynamic equilibrium melting temperature T_m. Maximizing ΔG with respect to r and l gives the free energy barrier

$$\Delta G^* = 8\pi \frac{{\sigma_s}^2 \sigma_e}{(\Delta G_v)^2} \tag{5}$$

The critical nucleus size, measured in the number of beads, is

$$n^* = 16\pi \rho_n \frac{{\sigma_s}^2 \sigma_e}{(\Delta G_v)^3} \tag{6}$$

Several methods have been developed to characterize the nucleation process from molecular dynamics (MD) simulations. The approach by Wedekind et al.[43] makes particularly clear the link between the classical theoretical treatment and the quantities available by MD simulation. This method has been successfully applied to the simulation of nucleation in *n*-alkanes before[42,44] and is employed here. According to this method, the mean first-passage time (MFPT) is the elapsed time of forming the largest nucleus in the system. As long as the critical free energy is relatively high ($\Delta G^* \gg k_B T$), the MFPT of the largest nucleus size, $\tau(n_{max})$, takes the following form

$$\tau(n_{max}) = 0.5\tau^*\{1 + \mathrm{erf}[Z\sqrt{\pi}(n_{max} - n^*)]\} + 0.5G^{-1}(n_{max} - n^*)[1 + \mathrm{erf}(C(n_{max} - n^*))] \tag{7}$$

where τ^* is the average incubation time, n^* is the critical nucleus size, G is the growth rate, Z is the Zeldovich factor, and C is a large positive fitting parameter. The second term on the right-hand side accounts for finite crystal growth rates of postcritical nuclei. This method allows us to estimate n^* and τ^* from MD simulations. Then after inserting n^* into eq 6, ${\sigma_s}^2\sigma_e$ will be obtained. Because ${\sigma_s}^2\sigma_e$ is directly related to the free energy barrier (eq 5), we use ${\sigma_s}^2\sigma_e$ as an indication of interfacial free energy. More details about this method are described in Wedekind[43] and Rutledge.[42]

2.5. Analysis of Molecular Topology. In order to quantify the crystallinity as well as the size distribution of crystallites, our previous work has provided a novel algorithm[28] based on hierarchical clustering. In this way, we are able to detect all crystal clusters (i.e., crystallites). If the size of a cluster is too small, clearly it is not stable and cannot be treated as a crystallite. We have done some statistics on the size distribution of clusters, and we found that clusters with size less than 50 units are unstable over time. Moreover, at the end of isothermal treatment, where the crystallization has been fully achieved, very few clusters with size from 50 to 1000 have been detected. There are mainly big crystallites (>1000) and small nuclei (<50), which are far below the critical size. In other words, large orientation clusters tend to form in the process of isothermal crystallization. Evidently, small and unstable clusters are not as important as big ones, and it is not wise to pay much attention on small clusters. As a consequence, we set the critical size of crystallites as 50, and clusters with less than 50 units would be treated as an amorphous phase.

Regarding structure−mechanical property relationships, a very important aspect is the molecular topology (essentially the

DOI: 10.1021/acs.macromol.9b00071
Macromolecules XXXX, XXX, XXX−XXX

number density of loop, tie, and cilia segments, see Figure 2). A topological segment is constituted by at least three units.

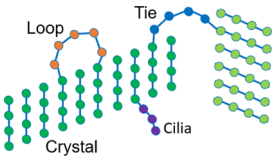

Figure 2. Schematic description of the possible polymer chains going in and out of crystallites: loop (orange), tie (blue), and cilia (purple). Green and dark green are crystal segments in two different crystallites.

Segments of less than three units would be treated as a flaw and integrated to the segments ahead and behind it. No loop with size less than three units has been detected. Loop, tie, and cilia have a size equal or higher than three. Apart from the molecular topology, sometimes we also need to mention a crystal segment in our following analysis, which is a crystal stem across the edges of the crystallite (see Figure 2).

In this work, more features will be added in our new algorithm to analyze the molecular topology of the systems.

Thanks to the molecular dynamics (MD) simulation, which makes it possible to trace every single chain units going in and out of crystallites, we propose a novel numeral topology algorithm to evaluate the molecular topology of the systems defined above. On the basis of the definition of the molecular topology as mentioned above, loop, tie, and cilia segments can be detected based on the trajectories of chain segments attached to the outer surfaces of crystallites. Only one exception happens because of the periodic conditions of MD simulations. From Figure 3, we can see that crystallites 1 and 2

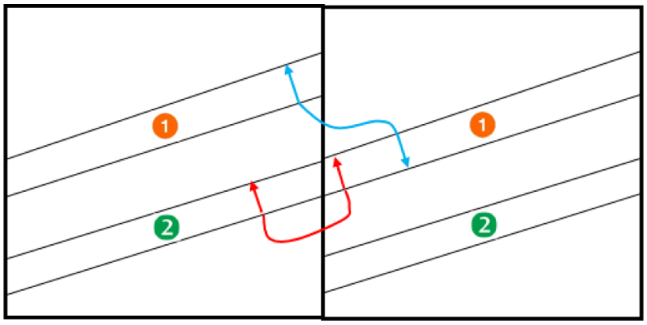

Figure 3. Scheme of a particular case because of periodic conditions of the simulation. Blocks 1 and 2 are crystallites. The blue chain segment is actually a tie, and the red one is a loop.

are actually one crystal because they are periodically connected. In this case, both the blue and red segments go back to the same crystallite and could therefore be considered as a loop. However, the blue segment is better described as a tie. In order to detect this particular case, we consider two vectors at the ends of a segment entering the same crystallite. If the vectors are in the same direction, it is a loop; if they are in the opposite direction, it is a tie. Consequently, all the segments of molecular topology and their sizes are unambiguously recorded for further studies.

3. RESULTS AND DISCUSSION

3.1. Isothermal Crystallization. As explained in Section 2, seven systems of uni- and bimodal polymers have been built, semicrystalline polymers have been obtained, and analysis of the crystallites and molecular topology has been performed. In this section, we evaluate the ability of these systems to crystallize.

3.1.1. MSID and Rouse Time. Figure 4 shows the MSID after the relaxation of $5 \times 10^5\tau_u$ at $T = 3.3\epsilon_u/k_B$. The convergence of MSID curves indicates that all the seven systems are well equilibrated after a period of $5 \times 10^5\tau_u$ relaxation. There are poor statistics for system LC10, as expected, because of relatively smaller number of long chains. In this process of evolution, the end-to-end vector orientation autocorrelation function $(\langle \mathrm{Ree}(t)\cdot\mathrm{Ree}(0)/(|\mathrm{Ree}(t)|\cdot|\mathrm{Ree}(0)|)\rangle)$ has also been obtained to calculate the Rouse time.[42,45] These results are shown in Figure 4d. From autocorrelation function versus time, a characteristic relaxation time is obtained. This relaxation time corresponds to the Rouse time τ_R, with the assumption that hydrodynamic interactions are screened in the melt. The inset of Figure 4d shows that the Rouse time increases dramatically with the weight fraction of long chains. In addition, the Rouse times of systems LC50 and LC70 are comparable with their incubation time (Figure 8a). We have quite fast nucleation here. Rutledge et al.[42] have also found the consistence of Rouse time and incubation time in the homogeneous nucleation of PE when the chain length is 150 CH_2 groups.

3.1.2. Overall Crystallization and Crystallinity. During the cooling stage from $T = 3.3$ to $2.3\epsilon_u/k_B$, the enthalpy varies linearly with time (see Figure 5a), indicating that crystallization is negligible. During the isothermal process at $2.3\epsilon_u/k_B$, after an incubation time, crystallization starts and the enthalpy goes down smoothly. The relatively high melting temperature, the significant melting enthalpy, as well as the continuous decrease of enthalpy during crystallization are a strong evidence of the thermodynamic stability of the crystal phase for all studied systems. The whole isothermal process lasts for $4 \times 10^5\tau_u$, and the enthalpy of all the systems reaches a plateau. At this point, all the systems have achieved the maximum of crystallization. Note that system LC100, consisting of only long chains, did not crystallize within the fixed isothermal time of $4 \times 10^5\tau_u$, suggesting that this system is much more difficult to crystallize compared with the other pure short-chain and bimodal MWD systems. In the following discussion, we mainly focus on the six crystallized systems. In Figure 5b–e, we also provide four snapshots in the process and at the end of crystallization for systems LC0 and LC50. Large lamellae with tapered edge have been obtained. Yamamoto[46] has also reported tapered shape lamellae between two parallel substrates using the CG model.

In order to calculate the achieved crystallinity, we use two methods. The first method is based on the experimental approach on isothermal crystallization.[47] The crystallinity is defined as

$$X_C = -\frac{\Delta H_c}{\Delta H_f^0} \tag{8}$$

where ΔH_c is the enthalpy of crystallization and ΔH_f^0 is the melting heat of the completely crystalline materials at the equilibrium melting temperature T_m^0. ΔH_f^0 has been calculated in our previous work[28] during melting, yielding $\Delta H_f^0 = 1.9\epsilon_u$. Figure 6 shows that the calculated crystallinity goes down from 0.66 to 0.46 with the weight fraction of long chains at the end of isothermal treatment because long chains make it more

DOI: 10.1021/acs.macromol.9b00071
Macromolecules XXXX, XXX, XXX−XXX

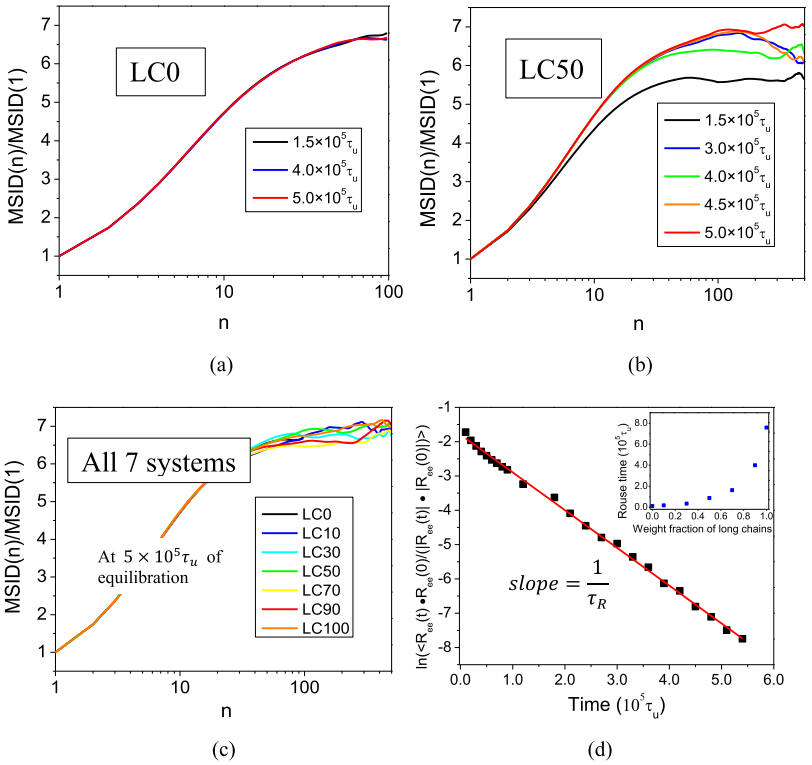

Figure 4. Evolution over time of MSIDs of polymer melts. (a) System LC0; (b) system LC50; and (c) all seven systems at the equilibration time of $5 \times 10^5\tau_u$. (d) End-to-end vector orientation autocorrelation function, $\langle \mathrm{Ree}(t)\cdot\mathrm{Ree}(0)/(|\mathrm{Ree}(t)|\cdot|\mathrm{Ree}(0)|\rangle$, for system LC50 melt at the relaxation temperature of $2.3\epsilon_u/k_B$. (Inset) Rouse time as a function of weight fraction of long chains for the simulated polymer melts.

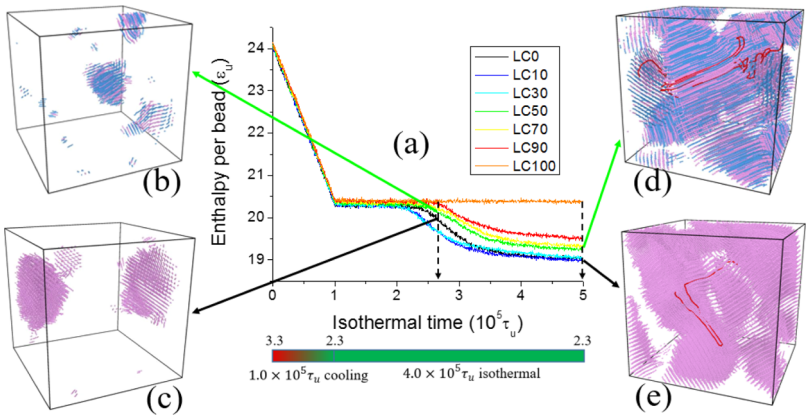

Figure 5. (a) Thermogram starting from the equilibrated liquid phase, cooling down from T = 3.3 to $2.3\epsilon_u/k_B$ and isothermal relaxation at T = $2.3\epsilon_u/k_B$. (b,c) Snapshots of systems LC50 and LC0 at the time of $2.65 \times 10^5\tau_u$. (d,e) Snapshots of systems LC50 and LC0 at the end of isothermal crystallization. The colors in snapshots: pink is the crystal atom of short chains, blue is the crystal atom of long chains, and red is a typical chain spanning crystalline and amorphous phases.

difficult for the polymer chains to crystallize from the entangled melts. This is consistent with Li et al.[48] who reported that the crystallization enthalpy (ΔH_c) would decrease with the increased molecular weight. Krumme et al.[21] have also drawn a conclusion that the fully achieved crystallinity decreases linearly with the molecular average weight in their experimental study of bimodal MWD PE. Moreover, Triandafilidi et al.[49] have found a faster decrease of crystallinity with the chain length of monodisperse polymer melts in MD simulations.

Nevertheless, there are distinct crystal characteristics of the polymer compared with other materials. Measurement of the density and other properties of polymer crystals have shown that they are not perfect crystals. The density of the crystals is always less than the theoretical density, which means that the noncrystalline material must also be present in the crystal. It is clear that crystalline polymers are by no means perfect from a structural viewpoint (defects with chain fold). They contain crystalline and amorphous regions and probably also areas, which are partially disordered. The method of eq 8 is a result of enthalpy change, which incorporates crystallization and defects. It is not a geometrical crystal and amorphous analysis. On the other hand, to detect the molecular topology of the semicrystalline system, we also need to locate the geometrical crystals to trace the chains going back and forth of the crystallites.

DOI: 10.1021/acs.macromol.9b00071
Macromolecules XXXX, XXX, XXX−XXX

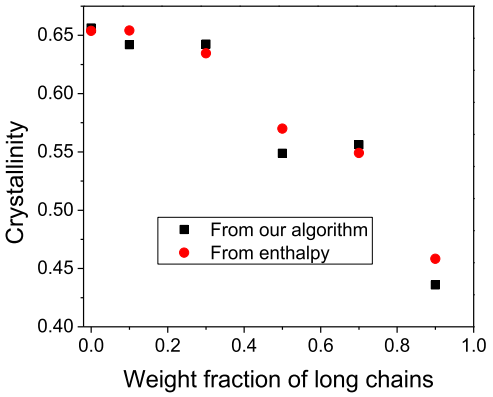

Figure 6. Calculated crystallinity from enthalpy and the hierarchical clustering method vs weight fraction of long chains.

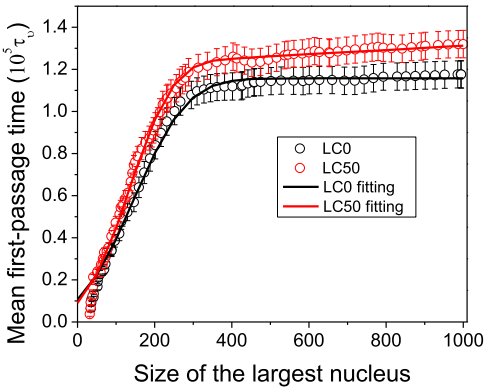

Figure 7. MFPT of maximum nucleus size (n_{max}) and fitting curves of function 7.

Given this, we have proposed the hierarchical clustering method, as illustrated in Section 2.5, to calculate crystallinity using our algorithm. A comparison of the two methods is shown in Figure 6. It is clear that the results are consistent. Thus, the algorithm illustrated in Section 2.4 will be used to analyze the topological structure of semicrystalline systems in the following sections.

3.1.3. Homogeneous Nucleation. The crystallization of a polymer arises from nucleation and crystal growth: the combination of these two processes dominates the crystallization rate. When the melt has been cooled completely, the nucleation starts and nuclei appear. Thermal fluctuations should be large enough in order to overcome the enthalpy barrier for nucleation. Once the nucleus is larger than the critical size, it will grow spontaneously as it will cause the Gibbs free energy to decrease.[50] According to CNT, the nucleation rate I is given by

$$I = A \exp\left(-\frac{E_d}{k_B T}\right)\exp\left(-\frac{\Delta G^*}{k_B T}\right) \quad (9)$$

where ΔG^* is the critical free energy barrier which mainly results from the interfacial free energy, E_d is the activation energy for chain mobility, and A is the temperature-independent factor. Equation 9 is not numerically used. Here, we demonstrate that at a given temperature, the nucleation rate depends on the interfacial free energy and the movement of chain segments. We will discuss the nucleation behavior of uni- and bimodal MWD systems in these two decisive perspectives.

The MFPT method of n_{max}, as explained in Section 2.4, is obtained using independent starting configurations for all the crystallized systems. Three trajectories for all the systems are collected. To be concise and explicit, here we only plot systems LC0 and LC50 (see Figure 7). Equation 7 is fitted to each of these curves, as shown in Figure 8a. Then we obtain the incubation time τ^* and the critical nucleus size n^*. After inserting n^* into eq 6, we can obtain the interfacial free energy $\sigma_s^2\sigma_e$. We plot incubation time (Figure 8a) and interfacial free energy $\sigma_s^2\sigma_e$ with critical nucleus size n^* (Figure 8b) versus weight fraction of long chains.

The incubation time τ^* is the time elapsed before the establishment of steady-state nucleation in the bulk. The nucleation rate I is equal to the inverse of the product of the incubation time and the volume of the system:[51] $I = 1/(\tau^* \times V)$, where V is the volume of the system. From Figure 8a, we can see that the incubation time varies between $0.9 \times 10^5\tau_u$ and $1.7 \times 10^5\tau_u$ for the six crystallized systems. It first decreases with the weight fraction of long chains, reaches a minimum at 30%, and then grows rapidly. System LC90 takes the longest time before the initiation of crystallization, whereas system LC30 takes the shortest time instead of LC0. Clearly, a bimodal MWD system would promote the nucleation of the isothermal process.

First of all, we explore the nucleation in the perspective of interfacial free energy. From Figure 8b, we can see that the interfacial free energy exhibits a drop from pure short-chain system LC0 to system LC10 with 10% of long chains. Then the interfacial free energy keeps going down until system LC90. According to eq 5, the free energy barrier would follow the same trend as interfacial free energy. Apparently, it turns out that the long-chain content would clearly promote the nucleation of the whole system in the perspective of free energy barrier. Song et al.[25] have also indicated that the high-molecular-weight component can lower the fold surface free energy (σ_e) of bimodal high-density PE (HDPE). They observed the promoted nucleation rate during the isothermal crystallization experiment and thereby concluded that the high-molecular-weight component may act as an effective nucleation agent in the HDPE matrix. Achilias et al.[52] have also indicated that long chains exhibit easier nucleation. We believe that the decreasing interfacial free energy could result from the role of chain folding in the process of nucleation.

Chainlike connection brings an intrinsic anisotropy to the shape of macromolecules, which favors parallel packing of the crystalline states.[53,54] Therefore, polymers can perform two typical modes of crystal nucleation: one is chain-folding configuration for a parallel alignment of consecutive strands along each chain, named *intramolecular* crystal nucleation. Another is the fringed-micelle configuration for a parallel alignment of several strands from different chains named *intermolecular* crystal nucleation,[53] as illustrated in Figure 9a. Flory[55] has estimated the free energy change of intermolecular nucleation of PE, and Zachmann found its stem-end surface free energy around 280 mJ/m^2.[56,57] In contrast, Hoffman and Miller estimated the fold-end surface free energy of PE around 90 mJ/m^2.[58] In the overcrowded surface of the fringed-micelle crystalline system, the amorphous segments would encounter a significant entropy loss. This can result in high-end surface free energy of fringed-micelle crystals. Because the interfacial free energy is responsible for the nucleation barrier, the chain-folding mode will have a much lower free energy barrier than

DOI: 10.1021/acs.macromol.9b00071
Macromolecules XXXX, XXX, XXX−XXX

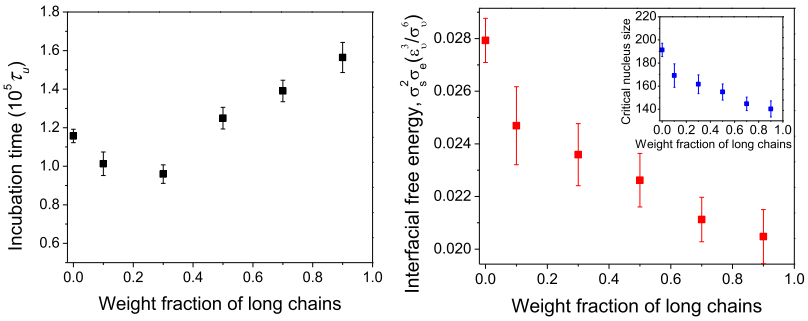

(a) (b)

Figure 8. (a) Incubation time vs weight fraction of long chains. (b) Calculated interfacial free energies vs weight fraction of long chains. (Inset) Critical nucleus size vs weight fraction of long chains.

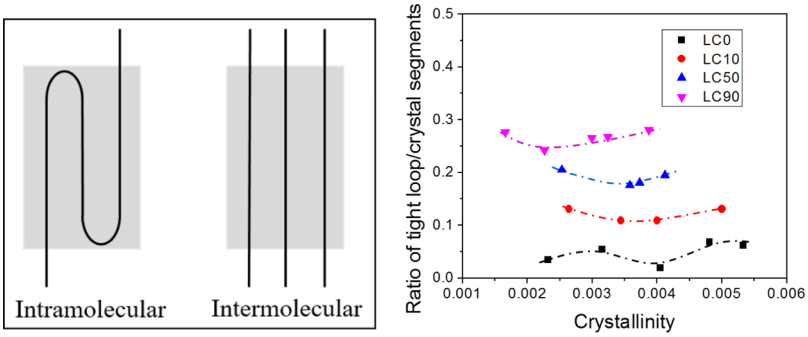

(a) (b)

Figure 9. (a) Illustration of intramolecular chain-folding mode and intermolecular fringed-micelle mode of crystal nucleation of polymers. (b) Ratio ($\mathfrak{R}$) of the number of tight loops and crystal segments.

the fringed-micelle mode in both primary crystal nucleation and secondary crystal nucleation. There always exists a competition between two modes of crystal nucleation during polymer crystallization.

As we can see in Figure 9a, intramolecular nucleation occurs when a chain forms a tight loop. In this case, the fold-end surface free energy will be lower than that of the stem-end surface free energy. In order to determine the critical size of a tight loop, we have looked at the influence of the thickness of the interfacial region on the energy per bead. It turns out that the energy per bead is influenced by the interface up to a distance of five bonds and that it remains constant for larger distances. This is also consistent with the LJ cutoff radius which is in our case approximately equal to $5\sigma_u$. From this analysis, we set the critical length of a tight loop as 11 beads. We have found that the majority of loops are tight ones. Meyer and Müller-Plathe[59] used a simplified version of model for poly(vinyl alcohol) and also found that most chains reenter the same lamellar region by a tight loop, resulting in chain-folded lamellae of polymer crystals.

By inspecting Figure 9a, we see that the intramolecular nucleation of a tight-folded chain gives rise to either one tight loop with two crystal segments or two tight loops and three crystal segments so that the ratio $\mathfrak{R}$ between the number of tight loops and crystal segments will be $\mathfrak{R} = 1/2$ or higher $\mathfrak{R} = 2/3$ in this case. For the intermolecular nucleation, there are no tight loops so that $\mathfrak{R} = 0$. In this way, we can establish the occurrence of intra- or intermolecular nucleation by quantifying the ratio $\mathfrak{R}$ between the number of tight loops and crystal segments.

Thanks to our algorithm explained in Section 2.5, we are able to calculate the ratio $\mathfrak{R}$ of the tight loop/crystal in the process of nucleation. In Figure 9b, we plot the ratio $\mathfrak{R}$ of the tight loop/crystal in the nucleation process. For clarity, we only plot four crystallized systems instead of six. We can see that the ratio $\mathfrak{R}$ for system LC0 is very close to 0, which indicates that intermolecular nucleation dominates system LC0. This ratio $\mathfrak{R}$ gradually increases to system LC90, showing that the chain-folded nucleation becomes important as the weight fraction of long chains increases. Figure 9b shows what happens during the nucleation process (before growth), where the crystallinity is very low. In this regime, crystallinity may fluctuate with time. In the nucleation process, the ratio of tight loop over crystal segments is fairly constant with crystallinity, and the different systems clearly exhibit different ratios, leading to different nucleation mechanisms (intra- or intermolecular nucleation, see Figure 9a). However, this ratio is totally in different situations during the crystal growth and at the end of the crystallization, which results from crystal thickening and growth mechanisms.

In some MD simulations,[60,61] researchers assumed that only intramolecular nucleation happens in their monodisperse polymer system, and they have concluded that the free energy barrier is independent of chain length. In some experimental works,[62,63] it has also been concluded that the free energy barrier for nucleation is independent of molar mass. Umemoto et al.[64] have also reported that there is a transition from intermolecular to intramolecular nucleation when the molecular weight is increased to around 3000 Da. According to these experimental and numerical works, it is believed that the free energy barrier of unimodal polymers is insensitive to molecular

DOI: 10.1021/acs.macromol.9b00071
Macromolecules XXXX, XXX, XXX−XXX

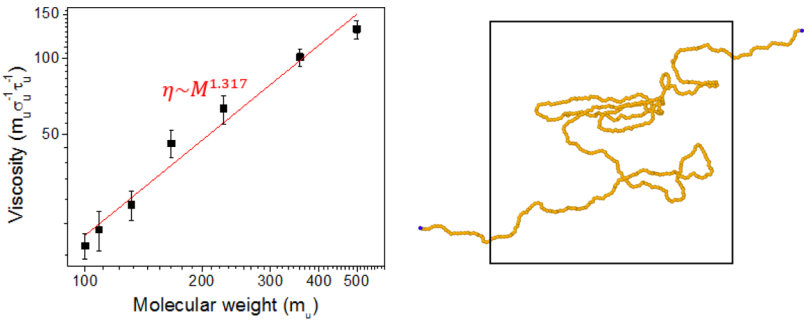

Figure 10. (a) Shear viscosity with average molecular weight, with the shear rate around $9.5 \times 10^{-3}\tau_u^{-3}$ and at the isothermal temperature of $2.3\epsilon_u/k_B$. (b) Configuration of individual long chains under the shear rate of system LC50.

weight within the intramolecular nucleation region (i.e., long-chain region) and within the intermolecular nucleation region (i.e., short-chain region) but differs between the two regions.

In the current work, we have used a chain length of 500 beads and 100 beads. According to Figure 9b, the ratio of tight loop/crystal segments of system LC0 (100-bead length) is very close to zero, which indicates that the intermolecular nucleation dominates. In systems LC10/LC50/LC90, this ratio increases with the rising content of long chains (500 beads). Therefore, the chain length 100 is in the intermolecular nucleation region and that of 500 is in the intramolecular nucleation region. Consequently, in our bimodal systems, the interfacial free energy variation results from a competition between inter- and intramolecular nucleation. Then the decreasing interfacial free energy with the weight fraction of long chains results from the rising fraction of chain-folded nucleation.

Even if the quantitative details of the results could depend on the specific values of the chain lengths used for our bimodal systems, the same general conclusions would still hold as long as the two types of chains are in intra- and intermolecular nucleation regions, respectively.

MD simulations[60,61] have suggested that the free energy barrier for nucleation in single polymers is independent of chain length in the intramolecular nucleation region. Experimental works[62,63] on the primary nucleation of PE also reported that the free energy barrier for nucleation is independent of molar mass within the intermolecular nucleation and intramolecular nucleation, respectively. Indeed, it seems that the intramolecular nucleation and intermolecular nucleation are insensitive to chain length. Hence, we believe that the decreasing interfacial free energy with the weight fraction of long chains results from the rising fraction of chain-folded nucleation.

Afterward, we explore the nucleation in the perspective of the movement of chain segments. In eq 9, E_d is the activation energy for processes that transport chain segments. Here, we include shear viscosity η as an indicator of E_d.

Nucleation is a very complex process because each polymer should be transported and rearranged under the strong restriction that the molecular chain must not be "cut". Nishi et al.[62] reported that the primary nucleation is a process of "chain sliding diffusion" within the nucleus, which requires disentanglement of molecular chains. It is also natural to consider that the chain sliding diffusion and disentanglement become more difficult with an increase in molecular weight. As a matter of fact, in nucleation and crystal growth, polymer chains are highly sheared and slightly disentangled at the local growth front. Instead of estimating zero-shear viscosity, we believe that a shear viscosity is more meaningful in exploring chain movements in the process of nucleation.

We calculate the shear viscosity with the reverse non-equilibrium MD (RNEMD) method of Müller-Plathe.[65] Compared to the traditional NEMD techniques, the main advantage of RNEMD is the fact that no energy is added to the system, and hence, no energy needs to be removed by an external thermostat. By constantly swapping the largest momentum components in the $+x$ and $-x$ directions, a gradient $(\partial v_x/\partial z)$ of the x component of the melt velocity (v_x) is formed with respect to z direction. It is also denoted as the shear rate. The momentum flux $j_z(p_x)$ is the x component of the momentum p_x transported in the z direction per given time and per unit area. The shear viscosity η is also defined as $j_z(p_x) = -\eta(\partial v_x/\partial z)$. We obtained the shear viscosity for all the seven systems at the shear rate around $9.5 \times 10^{-3}\tau_u^{-1}$ at the isothermal temperature of $2.3\epsilon_u/k_B$ at the beginning of the isothermal treatment before the crystallization started. As in RNEMD, chain sliding and disentanglement would occur in the sheared systems, which also happen in the process of nucleation.

Figure 10a shows the shear viscosity as a function of the weight fraction of long chains at the isothermal temperature of $2.3\epsilon_u/k_B$. As in ref 66, the logarithmic shear viscosity increases linearly with average molecular weight. Evidently, viscosity jumps up fast with increasing weight fraction of long chains. It is widely accepted in the experiment and modeling[67,68] that the zero rate viscosity is proportional to the power α of molecular weight, $\eta_0 \propto M_w^{\alpha}$, where the exponent α is 1.0 for unentangled chains and 3.4 for entangled chains. In this work, we found that the shear viscosity $\eta \propto M_w^{1.317}$, which is reasonable because a proportion of chains disentangle and align as mentioned above in the process of shearing. Figure 10b shows the configuration of a disentangled single long chain of system LC50 under the shear rate. This indicates that the polymer chains are somehow disentangled in the process of shearing, which accounts for the depression of power-law exponent.

According to eq 9, E_d, the activation energy for the movement of chain segments would be highly promoted as the weight fraction of long chains goes up. As a result, the nucleation rate will decrease. From this analysis, increasing the weight fraction of long chains results in two conflicting effects in the nucleation rate: promotion of interfacial free energy and decrease of chain diffusion. Interestingly, as we have seen for the incubation time in Figure 8a, the interfacial free energy

DOI: 10.1021/acs.macromol.9b00071
Macromolecules XXXX, XXX, XXX−XXX

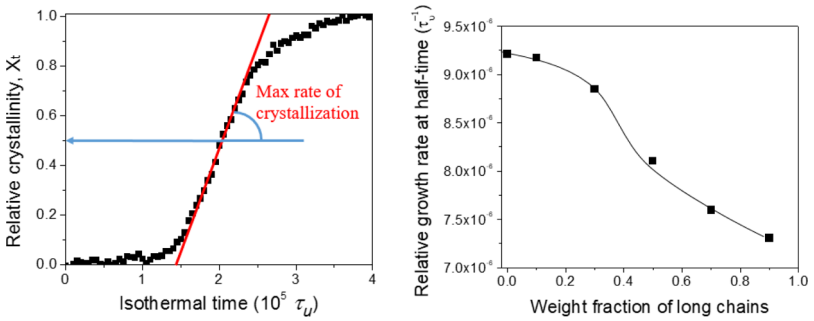

Figure 11. (a) Relative crystallinity of system LC50 with isothermal time and definition of maximum rate of crystallization. (b) Relative growth rate at half-time of crystallization as a function of weight fraction of long chains.

dominates the low M_w part and then reaches a minimum value at 30% of long chains. Afterward, the incubation time increases continuously, whereas the viscosity increases and then dominates the nucleation.

Some experimental studies[63,69] of polymer crystallization have been used to argue that the nucleation rate is inversely proportional to the molecular weight. Gee and Fried[70] have also reported that the time required for the onset of nucleation decreases with the number of monomers in the polymer. Essentially, long chains help in the formation of critical nuclei for short chains. When blending a small proportion of long chains (under 30% in our case), the free energy barrier strongly decreases because of reduced interfacial free energy, whereas the movement of chain segments is just slightly lowered. We have provided insights into how the bimodal MWD polymer promotes both nucleation and processability.

3.1.4. Crystal Growth. As explained above, we can calculate crystallinity at any time by the decrement of enthalpy using eq 8. We make the approximation that the relative crystallinity X_t equals crystallization divided by the fully achieved crystallinity within our isothermal time of $4 \times 10^5 \tau_u$. The relative degree of crystallinity (X_t) of system LC50 versus crystallization time at the isothermal temperature is plotted in Figure 11a. The tangent line at $X_t = 0.5$ is plotted: the gradient slope of this line is equal to the maximum rate of crystallization, which is an indication of general crystallization rate.[71]

We have obtained the maximum rate of crystallization for all the six crystallized systems and plotted versus different fractions of long chains, as presented in Figure 11b. In contrast to the nucleation rate, the growth rate decreases continuously with the weight fraction of long chains. The growth rate goes down slowly at the beginning and then undergoes an abrupt drop around 40% of long chains, after that the growth rate keeps decreasing fast until the end. Gee and Fried[70] have also reported that the growth rate of the crystal decreases with the number of monomers in the polymer. It turns out that the transport activation energy dominates the maximum rate of crystallization. However, from system LC0 to LC90, the molecular weight increases by 3.57 times and the maximum rate of crystallization only decreases by 20%. Evidently, there are other factors that could also influence the crystallization rate, such as surface free energy, thickness of crystallite, and melting enthalpy,[41,72] which we do not consider in this work. Nevertheless, we believe that bimodal MWD is also another key factor that influences the crystallization rate. Krumme et al.[21] and Shen et al.[31] have both found that the crystallization half-time is not strongly changed with increasing molecular weight in their studies of bimodal MWD PE.

3.2. Molecular Topology: Tracing Back to the Same Crystallinity (X_c = 43%). It was suggested that the chain topology that governs the distribution of the stress at a local scale on the crystalline lamella surface plays a major role in the propagation of microcracks from which are formed the crystal blocks.[26] Obviously, we are not able to compare the topology of the different systems because of the different crystallinities. Therefore, we assume that we can compare the chain topology if we trace all the systems back to the same crystallinity. We use system LC90 as a reference because it has the lowest crystallinity (43%) at the end of the crystallization: we analyze the topology of all the systems at this value of the crystallinity.

In order to link the topological state to the crystallinity, we performed extended isothermal MD steps for system LC50 after the end of the crystallization. We can see from Figure 12

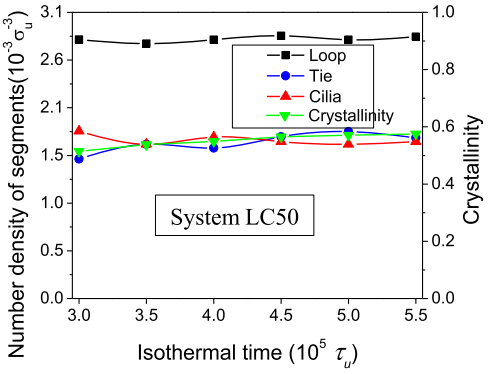

Figure 12. Extended isothermal crystallization procedure of system LC50.

that from $3 \times 10^5 \tau_u$ to $5.5 \times 10^5 \tau_u$, the crystallinity is almost constant and the molecular topology also slightly fluctuates around a plateau. This suggests that the topology does not significantly change if the crystallinity has saturated. On the basis of the results of Figure 12, we have reasons to speculate that crystallinity is representative of the corresponding topology (loop, tie, cilia). Given this speculation, we traced the systems back to the same crystallinity of around 43% and compare their topology.

Figure 13 shows the molecular topology (loop, tie, cilia) for different weight fractions of long chains of all the systems at the same crystallinity (43%). We can see that the number density of loops (Figure 13a) approximately increases with

DOI: 10.1021/acs.macromol.9b00071
Macromolecules XXXX, XXX, XXX−XXX

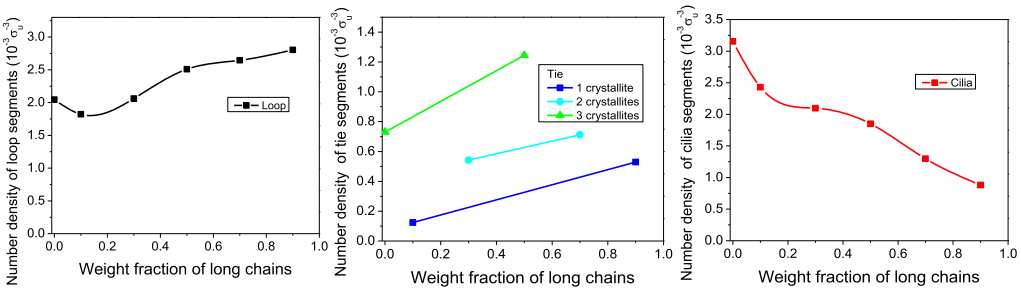

Figure 13. Molecular topology of six crystallized systems: comparison at the same crystallinity of 43%. Number density of (a) loop, (b) tie, and (c) cilia as a function of weight fraction of long chains.

long-chain fraction. This results from the increasing chain length. Clearly, long chains are more likely to go out of a crystallite and fold back to the same one, forming loop segments. Besides, we argue that the number of crystallites is also a factor that promotes the formation of loops. This would explain the drop of the loop curve at the beginning. There are three crystallites in system LC0 while only one in system LC10. Even with a shorter chain length, LC0 has more loop segments than LC10.

Tie segments play an important role in mechanical properties, fracture toughness, and resistance to slow crack growth of semicrystalline polymers. Previous research has proved[9] that the thickness of the amorphous layer (L_a) has a stronger impact than the crystal thickness (L_c) on the tie chain concentration. In other words, the distance between crystallites is a key factor for the formation of tie segments. In our systems, there are different numbers of crystallites in the simulation box, resulting in different distances between crystallites. It is reasonable to compare the number density of tie segments between systems with the same number of crystallites (see Figure 13b). In our systems with the same number of crystallites, tie segments also increase with long-chain weight fraction. Fundamentally, longer chains are more probable to span the amorphous phase and connect two crystallites. The probability of forming tie molecules decreases with increasing L_a.[3,73] As for cilias, it is clear that the number density decreases from LC0 to LC10. Because the number of chains also decreases from LC0 to LC10, consequently the number density of chain ends also decreases, leading to the reduced probability of forming cilias.

Lee and Rutledge[74−76] created semicrystalline samples with alternate crystal and amorphous stacks. In addition, the noncrystalline regions were subjected to equilibration by an interphase MC method that included both local rearrangements and alterations of chain topology. Out of the total number density of loop/tie/cilia segments in our simulations, the loop segments vary between 34.5 and 66.5% and the cilia segments vary between 53.2 and 20.9% from system LC0 to LC90 at the crystallinity of ∼43%, whereas Rutledge et al.[75] obtained 63.9% of loops and 33.3% of cilias in their systems at the average crystallinity of 53.7%. Higuchi and Kubo et al.[77] have also built CG models with a chain length of 1000 beads, where forces were applied to promote crystallization. They obtained 43.1% of loops in average at the crystallinity of 76%, with more percentage of ties and less cilias than in the current work. Compared with the study of Kubo et al., the lower percentage of tie segments and increase of cilia segments could be attributed to the short chains in our systems.

Figure 14 shows the average thickness of crystallites for all the simulation systems at the same crystallinity of 43%. When

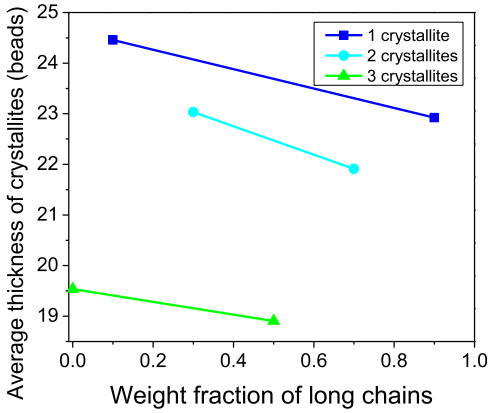

Figure 14. Average thickness of crystallites for six simulation systems: comparison at the same crystallinity of 43%.

it comes to MD simulation, the boundary effect would be a key factor for crystal thickness because the small distance between crystallites would hinder crystal thickening. Similar to the tie segment case discussed above, it is also reasonable to compare the average thickness of crystallites between systems with the same number of crystallites (see Figure 14). We can see that the average thickness drops from the 1-crystallite case to 3-crystallite case, proving the evident boundary effect of MD simulation. This phenomenon is opposite to the behavior of the number density of tie chains (see Figure 13b) which are promoted by the number of crystallites instead. For the situations with the same number of crystallites, the average thickness decreases with long-chain content. It seems that the crystal thickness is promoted by the short-chain content, which happens to be the inverse of the number density of tie segments (Figure 13b). This conclusion is consistent with experimental results[9,78] in a certain range. Sun et al.[78] found that the lamella thickness increased with the short-chain content in their crystallization studies of bimodal blends. Fujiwara and Sato[79] indicated that lamellar thickening growth occurred through chain sliding diffusion, which is the sliding motion along the chain axes.

4. CONCLUSIONS

In this study, we have investigated the crystallization and molecular topology of the bimodal MWD polymer by MD simulation. We have found that the incubation time of

DOI: 10.1021/acs.macromol.9b00071
Macromolecules XXXX, XXX, XXX−XXX

nucleation decreases with the rising weight fraction of long chains and that the long-chain content has opposite effects on nucleation in the perspective of interfacial free energy and chain segment diffusion. The interfacial free energy decreases with the weight fraction of long chains, which is attributed to the competition of chain-folded and chain-extended nucleation. We have provided insights into how the bimodal MWD polymer promotes both nucleation and processability, which has been rarely addressed before.

Furthermore, we have proposed a novel hierarchical clustering method to quantitatively access the molecular topology of semicrystalline systems. It has been proved that the number of loop and tie segments increases with the rising weight fraction of long-chain content. Topological features such as the tie segment population in semicrystalline polymers are believed to play an important role in the mechanical properties, whereas direct experimental measurement of the molecular topology is not easy, especially during deformation. However, there are already a few frontier research studies[74−77] that have addressed the effect of molecular topology on mechanical properties by MD simulation. It has been found that an increase in stress transmitters, which are molecular networks, such as tie segments and bridging entanglements, increases the yielding stress and decreases the generation of voids. As expected, bridging entanglements are stretched, and these persistent bridging entanglements behave similar to tie segments during deformation. However, the evolution of molecular topology in the process of semicrystalline polymer deformation would also be very interesting, and it has never been investigated to the best of the authors' knowledge. Further work on this point can enhance the molecular understanding of the mechanical properties of bimodal MWD semicrystalline polymers.

AUTHOR INFORMATION

Corresponding Author

*E-mail: olivier.lame@insa-lyon.fr.

ORCID

Zengqiang Zhai: 0000-0003-3912-5663

Notes

The authors declare no competing financial interest.

ACKNOWLEDGMENTS

All the simulations were performed on the massively parallel computer P2CHPD of FLMSN (Fédération Lyonnaise de Modélisation et Sciences Numériques). The Chinese Scholarship Council is acknowledged for the grant of a doctoral fellowship to Zengqiang ZHAI.

REFERENCES

(1) Patlazhan, S.; Remond, Y. Structural Mechanics of Semicrystalline Polymers Prior to the Yield Point: A Review. *J. Mater. Sci.* **2012**, *47*, 6749−6767.

(2) He, X.; Wang, Y.; Wang, Q.; Tang, Y.; Liu, B. Effects of Addition of Ultra-High Molecular Weight Polyethylene on Tie-Molecule and Crystallization Behavior of Unimodal PE-100 Pipe Materials. *J. Macromol. Sci. Part B-Physics* **2016**, *55*, 1007−1021.

(3) Seguela, R. Critical Review of the Molecular Topology of Semicrystalline Polymers: The Origin and Assessment of Intercrystalline Tie Molecules and Chain Entanglements. *J. Polym. Sci. Part B Polym. Phys.* **2005**, *43*, 1729−1748.

(4) Huang, Y.-L.; Brown, N. Dependence of slow crack growth in polyethylene on butyl branch density: Morphology and theory. *J. Polym. Sci. Part B-Polymer Phys.* **1991**, *29*, 129−137.

(5) García, R. A.; Carrero, A.; Martín, C.; Domínguez, C. Effects of the Structural Components on Slow Crack Growth Process in Polyethylene Blends. Composition Intervals Prediction for Pipe Applications. *J. Appl. Polym. Sci.* **2011**, *121*, 3269−3276.

(6) Kumar, V.; Locker, C. R.; in't Veld, P. J.; Rutledge, G. C. Effect of Short Chain Branching on the Interlamellar Structure of Semicrystalline Polyethylene. *Macromolecules* **2017**, *50*, 1206−1214.

(7) Nilsson, F.; Gedde, U. W.; Hedenqvist, M. S. Modelling the Relative Permittivity of Anisotropic Insulating Composites. *Compos. Sci. Technol.* **2011**, *71*, 216−221.

(8) Gautam, S.; Balijepalli, S.; Rutledge, G. C. Molecular Simulations of the Interlamellar Phase in Polymers: Effect of Chain Tilt. *Macromolecules* **2000**, *33*, 9136−9145.

(9) Nilsson, F.; Lan, X.; Gkourmpis, T.; Hedenqvist, M. S.; Gedde, U. W. Modelling Tie Chains and Trapped Entanglements in Polyethylene. *Polymer* **2012**, *53*, 3594−3601.

(10) Humbert, S.; Lame, O.; Séguéla, R.; Vigier, G. A Re-Examination of the Elastic Modulus Dependence on Crystallinity in Semi-Crystalline Polymers. *Polymer* **2011**, *52*, 4899−4909.

(11) Makke, A.; Lame, O.; Perez, M.; Barrat, J.-L. Influence of Tie and Loop Molecules on the Mechanical Properties of Lamellar Block Copolymers. *Macromolecules* **2012**, *45*, 8445−8452.

(12) Xiong, B.; Lame, O.; Chenal, J.-M.; Men, Y.; Seguela, R.; Vigier, G. Critical Stress and Thermal Activation of Crystal Plasticity in Polyethylene: Influence of Crystal Microstructure and Chain Topology. *Polymer* **2017**, *118*, 192−200.

(13) Strebel, J. J.; Moet, A. The Effects of Annealing on Fatigue Crack Propagation in Polyethylene. *J. Polym. Sci. Part B Polym. Phys.* **1995**, *33*, 1969−1984.

(14) Huang, Y.-L.; Brown, N. The Effect of Molecular Weight on Slow Crack Growth in Linear Polyethylene Homopolymers. *J. Mater. Sci.* **1988**, *23*, 3648−3655.

(15) Hubert, L.; David, L.; Séguéla, R.; Vigier, G.; Corfias-Zuccalli, C.; Germain, Y. Physical and mechanical properties of polyethylene for pipes in relation to molecular architecture. II. Short-term creep of isotropic and drawn materials. *J. Appl. Polym. Sci.* **2002**, *84*, 2308−2317.

(16) Zhang, S.; Zhao, N.; Wu, Y.; Dong, Q.; Wang, Q.; Tang, Y.; Yu, Y.; Da, J.; He, X.; Cheng, R. Short Chain Branches Distribution Characterization of Ethylene/1-Hexene Copolymers by Using TREF+ 13C-NMR and TREF+ SC Methods. In *Macromolecular Symposia*; Wiley Online Library, 2012; Vol. *312*, pp 63−71.

(17) Krishnaswamy, R. K.; Yang, Q.; Fernandez-Ballester, L.; Kornfield, J. A. Effect of the Distribution of Short-Chain Branches on Crystallization Kinetics and Mechanical Properties of High-Density Polyethylene. *Macromolecules* **2008**, *41*, 1693−1704.

(18) Lenzi, M. K.; Cunningham, M. F.; Lima, E. L.; Pinto, J. C. Producing Bimodal Molecular Weight Distribution Polymer Resins Using Living and Conventional Free-Radical Polymerization. *Ind. Eng. Chem. Res.* **2005**, *44*, 2568−2578.

(19) Li, W.; Guan, C.; Xu, J.; Chen, Z.-r.; Jiang, B.; Wang, J.; Yang, Y. Bimodal/Broad Polyethylene Prepared in a Disentangled State. *Ind. Eng. Chem. Res.* **2014**, *53*, 1088−1096.

(20) Krumme, A.; Lehtinen, A.; Viikna, A. Crystallisation Behaviour of High Density Polyethylene Blends with Bimodal Molar Mass Distribution 1. Basic Characteristics and Isothermal Crystallisation. *Eur. Polym. J.* **2004**, *40*, 359−369.

(21) Krumme, A.; Lehtinen, A.; Viikna, A. Crystallisation behaviour of high density polyethylene blends with bimodal molar mass distribution. *Eur. Polym. J.* **2004**, *40*, 371−378.

(22) Zuo, F.; Keum, J. K.; Yang, L.; Somani, R. H.; Hsiao, B. S. Thermal Stability of Shear-Induced Shish-Kebab Precursor Structure from High Molecular Weight Polyethylene Chains. *Macromolecules* **2006**, *39*, 2209−2218.

(23) Yang, L.; Somani, R. H.; Sics, I.; Hsiao, B. S.; Kolb, R.; Fruitwala, H.; Ong, C. Shear-Induced Crystallization Precursor

DOI: 10.1021/acs.macromol.9b00071
Macromolecules XXXX, XXX, XXX−XXX

Studies in Model Polyethylene Blends by in-Situ Rheo-SAXS and Rheo-WAXD. *Macromolecules* **2004**, *37*, 4845−4859.
(24) Shen, H.-W.; Luan, T.; Xie, B.-H.; Yang, W.; Yang, M.-B. Rheological Behaviors and Molecular Weight Distribution Characteristics of Bimodal High-Density Polyethylene. *J. Appl. Polym. Sci.* **2011**, *121*, 1543−1549.
(25) Song, S.; Wu, P.; Ye, M.; Feng, J.; Yang, Y. Effect of Small Amount of Ultra High Molecular Weight Component on the Crystallization Behaviors of Bimodal High Density Polyethylene. *Polymer* **2008**, *49*, 2964−2973.
(26) Humbert, S.; Lame, O.; Chenal, J.-M.; Seguela, R.; Vigier, G. Memory Effect of the Molecular Topology of Lamellar Polyethylene on the Strain-Induced Fibrillar Structure. *Eur. Polym. J.* **2012**, *48*, 1093−1100.
(27) Moyassari, A.; Mostafavi, H.; Gkourmpis, T.; Hedenqvist, M. S.; Gedde, U. W.; Nilsson, F. Simulation of Semi-Crystalline Polyethylene: Effect of Short-Chain Branching on Tie Chains and Trapped Entanglements. *Polymer* **2015**, *72*, 177−184.
(28) Morthomas, J.; Fusco, C.; Zhai, Z.; Lame, O.; Perez, M. Crystallization of Finite-Extensible Nonlinear Elastic Lennard-Jones Coarse-Grained Polymers. *Phys. Rev. E* **2017**, *96*, 052502.
(29) Brown, N.; Ward, I. M. The Influence of Morphology and Molecular Weight on Ductile-Brittle Transitions in Linear Polyethylene. *J. Mater. Sci.* **1983**, *18*, 1405−1420.
(30) Séguéla, R. On the Natural Draw Ratio of Semi-Crystalline Polymers: Review of the Mechanical, Physical and Molecular Aspects. *Macromol. Mater. Eng.* **2007**, *292*, 235−244.
(31) Shen, H.; Xie, B.; Yang, W.; Yang, M. Non-Isothermal Crystallization of Polyethylene Blends with Bimodal Molecular Weight Distribution. *Polym. Test.* **2013**, *32*, 1385−1391.
(32) Takeuchi, H. Structure Formation during the Crystallization Induction Period of a Short Chain-Molecule System: A Molecular Dynamics Study. *J. Chem. Phys.* **1998**, *109*, 5614.
(33) Fujiwara, S.; Sato, T. Molecular Dynamics Simulation of Structural Formation of Short Polymer Chains. *Phys. Rev. Lett.* **1998**, *80*, 991.
(34) Liu, Z. H.; Wang, C. S.; Wang, X. Q.; Huang, N. X.; Filippini-Fantoni, R. Monte Carlo Technique to Simulate Amide Interchange Reactions, 3. *Macromol. Theory Simulations* **2005**, *14*, 164−171.
(35) Tobita, H. Bimodal Molecular Weight Distribution Formed in the Emulsion Polymerization of Ethylene. *J. Polym. Sci. Part a-Polymer Chem.* **2002**, *40*, 3426−3433.
(36) Tobita, H. Bimodal Molecular Weight Distribution Formed in Emulsion Polymerization with Long-Chain Branching. *Polym. React. Eng.* **2003**, *11*, 855−868.
(37) Plimpton, S. Fast Parallel Algorithms for Short-Range Molecular Dynamics. *J. Comput. Phys.* **1995**, *117*, 1−19.
(38) Deiber, J. A.; Peirotti, M. B.; Gappa, A. The Linear Viscoelastic Relaxation Modulus Related to the MWD of Linear Homopolymer Blends. *J. Elastomers Plast.* **1997**, *29*, 290−313.
(39) Perez, M.; Lame, O.; Leonforte, F.; Barrat, J.-L. Polymer Chain Generation for Coarse-Grained Models Using Radical-like Polymerization. *J. Chem. Phys.* **2008**, *128*, 234904.
(40) Mahaud, M.; Zhai, Z.; Perez, M.; Lame, O.; Fusco, C.; Chazeau, L.; Makke, A.; Marque, G.; Morthomas, J. Polymer Chain Generation for Coarse-Grained Models Using Radical-Like Polymerization. *Commun. Comput. Phys.* **2018**, *24*, 885−898.
(41) Hoffman, J. D.; Weeks, J. J. Rate of Spherulitic Crystallization with Chain Folds in Polychlorotrifluoroethylene. *J. Chem. Phys.* **1962**, *37*, 1723−1741.
(42) Yi, P.; Locker, C. R.; Rutledge, G. C. Molecular Dynamics Simulation of Homogeneous Crystal Nucleation in Polyethylene. *Macromolecules* **2013**, *46*, 4723−4733.
(43) Wedekind, J.; Strey, R.; Reguera, D. New Method to Analyze Simulations of Activated Processes. *J. Chem. Phys.* **2007**, *126*, 134103.
(44) Anwar, M.; Berryman, J. T.; Schilling, T. Crystal Nucleation Mechanism in Melts of Short Polymer Chains under Quiescent Conditions and under Shear Flow. *J. Chem. Phys.* **2014**, *141*, 124910.
(45) Harmandaris, V. A.; Mavrantzas, V. G.; Theodorou, D. N. Atomistic Molecular Dynamics Simulation of Polydisperse Linear Polyethylene Melts. *Macromolecules* **1998**, *31*, 7934−7943.
(46) Yamamoto, T. Molecular Dynamics Simulation of Polymer Ordering. II. Crystallization from the Melt. *J. Chem. Phys.* **2001**, *115*, 8675.
(47) Kong, Y.; Hay, J. N. The Measurement of the Crystallinity of Polymers by DSC. *Polymer* **2002**, *43*, 3873−3878.
(48) Li, Z.; Zhang, W.; Feng, L.; Shen, X.; Mai, Y. Role of the Amorphous Morphology in Physical Properties of Ultra High Molecular Weight Polyethylene. *Polym. Plast. Technol. Eng.* **2014**, *53*, 1194−1204.
(49) Triandafilidi, V.; Rottler, J.; Hatzikiriakos, S. G. Molecular Dynamics Simulations of Monodisperse/Bidisperse Polymer Melt Crystallization. *J. Polym. Sci. Part B Polym. Phys.* **2016**, *54*, 2318−2326.
(50) Kocic, N.; Lederhofer, S.; Kretschmer, K.; Bastian, M.; Heidemeyer, P. Nucleation Parameter and Size Distribution of Critical Nuclei for Nonisothermal Polymer Crystallization: The Influence of the Cooling Rate and Filler. *J. Appl. Polym. Sci.* **2015**, *132* (). DOI: 10.1002/app.41433
(51) Kashchiev, B. D.; Heinemann, B. *Nucleation—Basic Theory with Applications Guide to Capital Cost Estimating*; Butterworth Heinemann: Oxford, Boston, 2000.
(52) Achilias, D. S.; Papageorgiou, G. Z.; Karayannidis, G. P. Isothermal and nonisothermal crystallization kinetics of poly(propylene terephthalate). *J. Polym. Sci. Part B Polym. Phys.* **2004**, *42*, 3775−3796.
(53) Hu, W. The Physics of Polymer Chain-Folding. *Phys. Rep.* **2018**, *747*, 1−50.
(54) Hu, W.; Frenkel, D. Polymer Crystallization Driven by Anisotropic Interactions. *Interphases and Mesophases in Polymer Crystallization III*; Advances in Polymer Science; Springer, 2005; pp 1−35.
(55) Flory, P. J. Thermodynamics of Crystallization in High Polymers. IV. A Theory of Crystalline States and Fusion in Polymers, Copolymers, and Their Mixtures with Diluents. *J. Chem. Phys.* **1949**, *17*, 223−240.
(56) Zachmann, H. G. Der Einfluß der Konfigurationsentropie auf das Kristallisations- und Schmelzverhalten von hochpolymeren Stoffen. *Kolloid-Zeitschrift und Zeitschrift für Polym.* **1967**, *216−217*, 180−191.
(57) Zachmann, H. G. Statistische Thermodynamik Des Kristallisierens Und Schmelzens von Hochpolymeren Stoffen. *Kolloid-Zeitschrift und Zeitschrift für Polym.* **1969**, *231*, 504−534.
(58) Hoffman, J. D.; Miller, R. L. Kinetic of crystallization from the melt and chain folding in polyethylene fractions revisited: theory and experiment. *Polymer* **1997**, *38*, 3151−3212.
(59) Meyer, H.; Müller-Plathe, F. Formation of Chain-Folded Structures in Supercooled Polymer Melts. *J. Chem. Phys.* **2001**, *115*, 7807.
(60) Hu, W.; Frenkel, D.; Mathot, V. B. F. Intramolecular Nucleation Model for Polymer Crystallization. *Macromolecules* **2003**, *36*, 8178−8183.
(61) Hu, W.; Frenkel, D.; Mathot, V. B. F. Free Energy Barrier to Melting of Single-Chain Polymer Crystallite. *J. Chem. Phys.* **2003**, *118*, 3455−3457.
(62) Nishi, M.; Hikosaka, M.; Ghosh, S. K.; Toda, A.; Yamada, K. Molecular Weight Dependence of Primary Nucleation Rate of Polyethylene I. An Extended Chain Single Crystal. *Polym. J.* **1999**, *31*, 749−758.
(63) Ghosh, S. K.; Hikosaka, M.; Toda, A. Power Law of Nucleation Rate of Folded-Chain Single Crystals of Polyethylene. *Colloid Polym. Sci.* **2001**, *279*, 382−386.
(64) Umemoto, S.; Kikutani, T.; Kawano, R.; Okui, N.; Hayashi, R. Molecular Weight Dependence of Primary Nucleation Rate of Poly(Ethylene Succinate). *J. Macromol. Sci. Part B* **2003**, *42*, 421−430.
(65) Chen, X.; Carbone, P.; Cavalcanti, W. L.; Milano, G.; Müller-Plathe, F. Viscosity and Structural Alteration of a Coarse-Grained

DOI: 10.1021/acs.macromol.9b00071
Macromolecules XXXX, XXX, XXX−XXX

Model of Polystyrene under Steady Shear Flow Studied by Reverse Nonequilibrium Molecular Dynamics. *Macromolecules* **2007**, *40*, 8087−8095.
(66) Byutner, O.; Smith, G. D. Temperature and Molecular Weight Dependence of the Zero Shear-Rate Viscosity of an Entangled Polymer Melt from Simulation and Theory. *J. Polym. Sci. Part B-Polymer Phys.* **2001**, *39*, 3067−3071.
(67) Shen, H.-W.; Xie, B.-H.; Yang, W.; Yang, M.-B. Thermal and Rheological Properties of Polyethylene Blends with Bimodal Molecular Weight Distribution. *J. Appl. Polym. Sci.* **2013**, *129*, 2145−2151.
(68) Nikoubashman, A.; Howard, M. P. Equilibrium Dynamics and Shear Rheology of Semiflexible Polymers in Solution. *Macromolecules* **2017**, *50*, 8279−8289.
(69) Kraack, H.; Deutsch, M.; Sirota, E. B. N-Alkane Homogeneous Nucleation: Crossover To Polymer Behavior. *Macromolecules* **2000**, *33*, 6174−6184.
(70) Gee, R. H.; Fried, L. E. Ultrafast Crystallization of Polar Polymer Melts. *J. Chem. Phys.* **2003**, *118*, 3827.
(71) Long, Y.; Shanks, R. A.; Stachurski, Z. H. Kinetics of Polymer Crystallisation. *Prog. Polym. Sci.* **1995**, *20*, 651−701.
(72) Sun, Y.; Matsumoto, M.; Haruki, M.; Kihara, S.-i.; Takishima, S. Molecular weight dependence of the crystallization of the polycarbonate induced by supercritical CO 2. *J. Supercrit. Fluids* **2016**, *113*, 144−149.
(73) Rastogi, S.; Lippits, D. R.; Höhne, G. W. H.; Mezari, B.; Magusin, P. C. M. M. The Role of the Amorphous Phase in Melting of Linear UHMW-PE; Implications for Chain Dynamics. *J. Phys. Condens. Matter* **2007**, *19*, 205122.
(74) Lee, S.; Rutledge, G. C. Plastic Deformation of Semicrystalline Polyethylene by Molecular Simulation. *Macromolecules* **2011**, *44*, 3096−3108.
(75) Kim, J. M.; Locker, R.; Rutledge, G. C. Plastic Deformation of Semicrystalline Polyethylene under Extension, Compression, and Shear Using Molecular Dynamics Simulation. *Macromolecules* **2014**, *47*, 2515−2528.
(76) Yeh, I.-C.; Andzelm, J. W.; Rutledge, G. C. Mechanical and Structural Characterization of Semicrystalline Polyethylene under Tensile Deformation by Molecular Dynamics Simulations. *Macromolecules* **2015**, *48*, 4228−4239.
(77) Higuchi, Y.; Kubo, M. Deformation and Fracture Processes of a Lamellar Structure in Polyethylene at the Molecular Level by a Coarse-Grained Molecular Dynamics Simulation. *Macromolecules* **2017**, *50*, 3690−3702.
(78) Sun, X.; Shen, H.; Xie, B.; Yang, W.; Yang, M. Fracture Behavior of Bimodal Polyethylene: Effect of Molecular Weight Distribution Characteristics. *Polymer* **2011**, *52*, 564−570.
(79) Fujiwara, S.; Sato, T. Molecular Dynamics Simulation of Structure Formation of Short Chain Molecules. *J. Chem. Phys.* **1999**, *110*, 9757.

DOI: 10.1021/acs.macromol.9b00071
Macromolecules XXXX, XXX, XXX−XXX